

ASCA observations of Seyfert 1 galaxies:

I. Data Analysis, Imaging and Timing

K. Nandra^{1,2}, I.M. George^{1,3}, R.F. Mushotzky¹, T.J. Turner^{1,3}, T. Yaqoob^{1,3}

ABSTRACT

We present the first in a series of papers describing the X-ray properties of a sample of 18 Seyfert 1 galaxies, using data obtained by *ASCA*. The imaging data reveal a number of serendipitous hard X-ray sources in some source fields, but none contribute significantly to the hard X-ray flux of the AGN. All but one of the Seyferts show evidence for variability on timescales of minutes-hours, with the amplitude anti-correlated with the source luminosity, confirming previous results. In at least 8 sources, there is evidence that the variability amplitude below 2 keV is greater than that in the hard X-ray band, perhaps indicating variable components other than the power-law in the soft band. Ultra-rapid variability, implying significant power at frequencies $> 10^{-3}$ Hz is detected in at least 5 sources, but is difficult to detect in most cases, due to the sampling and signal-to-noise ratio. In Mrk 766 and MCG-6-30-15 there is also an indication that the high-frequency power-spectra are variable in shape and/or intensity. There is similar evidence in NGC 4151, but on longer time scales.

Subject headings: galaxies:active – galaxies:nuclei – X-rays: galaxies

1. Introduction

The Ariel V and HEAO-1 surveys showed that the brightest class of active galactic nuclei (AGN) in the hard X-ray band are nearby, Seyfert 1 galaxies. Whilst it is unclear whether or not such sources are representative of the AGN phenomenon in general, the high signal-to-noise ratio enables them to be studied in most detail in the X-ray band.

¹Laboratory for High Energy Astrophysics, Code 660, NASA/Goddard Space Flight Center, Greenbelt, MD 20771

²NAS/NRC Research Associate

³Universities Space Research Association

Long term (days to years) variability is a property of these sources established early in the history of X-ray astronomy (e.g. Marshall, Warwick & Pounds 1981), with variations in amplitude of factors up to an order of magnitude being common. Only two sources showed evidence for more rapid variability in the HEAO-1 or *Einstein* data; NGC 4051 (Marshall et al. 1983) and NGC 6814 (Tennant & Mushotzky 1983). In the latter case, the variability is most likely to be due to a nearby cataclysmic variable (Madejski et al. 1993).

Long duration, uninterrupted X-ray observations of AGN were first afforded by *EXOSAT*, which showed that the previous lack of detection was due primarily to low signal-to-noise ratio and observation duration. *EXOSAT*'s highly elliptical orbit eliminated constraints due to earth occultation and SAA passage for up to 4 days. Examination of the light curves from short ($\sim 20,000$ sec) observations showed that rapid variability was common, contrary to the conclusions from low earth orbit satellites. (e.g., Lawrence et al. 1985; Pounds, Turner & Warwick 1986). In a study of a sample of 48 Seyfert galaxies, at least 30% showed clear rapid X-ray variability (Turner 1988).

EXOSAT also provided the first evenly-sampled light curves of AGN, and therefore an opportunity to estimate the power-density spectrum (PDS) to reasonable accuracy. The PDS can be used to identify characteristic time scales in the variability, which might be related to physical sizes in the source. However, early efforts showed scale-invariant variability, with a $f^{-\alpha}$ “red-noise” noise spectrum, possibly with $\alpha \sim 1$ (Lawrence et al. 1987; McHardy & Czerny 1987). Improved techniques have revealed further information. Lawrence & Papadakis (1993) reported on a series of *EXOSAT* “long-look” observations and found that the power-spectrum slopes were consistent with a mean values of $\alpha \sim 1.55 \pm 0.09$. Using different techniques, Green, McHardy & Lehto (1993) presented similar results for a larger sample and found $\alpha \sim 1.7 \pm 0.5$. However, both sets of authors presented evidence that the amplitude of the PDS depends on the source luminosity, confirming a similar result based on the doubling time scale given by Barr & Mushotzky (1986). Green et al. (1993) also reported that the low-energy (LE) power spectra of two sources were steeper than the medium-energy (ME) spectra. It is still unclear whether there are any characteristic time scales in the X-ray variability of AGN. With the best example of a periodicity - NGC 6814 - having evaporated, the strongest evidence is of quasi-periodic oscillations in the *EXOSAT* power spectra of NGC 5548 and NGC 4051 (Papadakis & Lawrence 1993, 1995). These observations await confirmation with other satellites. Unfortunately, all the data taken since the demise of *EXOSAT* have been sampled unevenly. When combined with the relatively high Poisson noise level associated with sources of this strength, further progress in our knowledge of the power spectra has been severely hampered.

After introducing our sample in Section 2 and our analysis methods in Section 3, we

discuss the *ASCA* imaging data in Section 4. We demonstrate the hard X-ray emission we describe here is consistent with an origin in a point-like source centered on the optical galaxy and is therefore associated with the AGN, rather than some contaminating source. The time dependence of the X-ray emission of our Seyfert 1 galaxies is discussed in Section 5. Finally, we discuss our results in Section 6.

2. The Sample

Here we present an analysis of *ASCA* observations of Seyfert 1 galaxies performed prior to 1994 May 01. All such observations are now available in the public archives. We define Seyfert 1 galaxies as AGN at redshifts $z < 0.05$, with predominantly broad lines, as indicated by the Seyfert 1.0-1.5 classification. We recognize that these distinctions are somewhat arbitrary and that our sources do not comprise a complete sample. In the early stages of any mission, the tendency is for the brightest X-ray sources to be observed, hence our sample consists primarily of hard X-ray selected AGN from the HEAO-1 “Piccinotti sample” (Piccinotti et al. 1982). The majority have been studied extensively in the hard X-ray band by *HEAO-1* (Mushotzky et al. 1984), *EXOSAT* (Turner & Pounds 1989) and *Ginga* (Nandra & Pounds 1994). Analyses of higher-redshift and narrow-line AGN will be presented elsewhere. Our sample consists of 18 sources and is listed in Table 1. Histograms of the redshift and X-ray luminosity distributions are shown in Fig. 1. The luminosities were calculated assuming a power-law fit to the spectra, $H_0 = 50 \text{ km s}^{-1} \text{ Mpc}^{-1}$ and $q_0 = 0.5$.

As our intention is to study the mean properties of the sample we do not include a detailed discussion of individual sources. However, we note that many of these observations have been published in the literature already and the reader directed to the references noted in Table 2, and those therein, for analyses of the individual objects.

3. Data selection and analysis

Detailed information regarding *ASCA* and the analysis of data from that satellite can be found in Tanaka, Inoue & Holt (1994), Day et al. 1995 and references therein. Four co-aligned, grazing-incidence, foil-mirror telescopes (Serlemitsos et al. 1995) are employed to direct X-rays onto four focal-plane instruments simultaneously. There are two CCD detectors – the Solid-state Imaging Spectrometers (SIS; Gendreau 1995) and two gas-scintillation proportional-counters – the Gas Imaging Spectrometers (GIS; Tashiro et al. 1995).

Our *ASCA* SIS data were obtained in one of two data modes (known as **FAINT** and **BRIGHT**), one of three clocking modes (1,2 or 4-CCD modes) depending on the number of CCD chips being read out and one of three telemetry modes (**LOW**, **MEDIUM** and **HIGH** bit rates). A given observation invariably contains a mixture of these modes. Analysis of **FAINT** mode data alone allows correction for Dark Frame Error (DFE) and “echo” effects (Otani & Dotani 1994), which permits utilization of the maximum energy resolution of the instruments. However, they cannot then be combined with the **BRIGHT** mode data. Thus, if signal-to-noise ratio is a more important consideration than spectral resolution, the **FAINT** data can be converted into a format identical to the **BRIGHT** mode data and thus the two types of data can be combined. Combining data taken in different clocking modes can cause problems in the analysis, due to different background and CCD zero-levels and are generally not combined. In principle telemetry modes can be combined.

The vast majority of the GIS data described here were taken in so-called **PH** mode, which provides the maximum energy and spatial resolution.

Our data were obtained from the US public archive (located at the HEASARC, NASA/GSFC). Table 2 shows the observation catalog. A total of 30 observation were made of our sources, where we define an “observation” as a distinct dataset within the archive. The starting point for our analysis were the “raw” event files from the database. These were created from the original telemetry file and have been corrected to produce linearized detector coordinates, gain corrected pulse-height values and sky co-ordinates determined from the spacecraft attitude. Furthermore, the SIS **FAINT** data have been converted to both **BRIGHT** mode format and an alternative form corrected for DFE and echo effects, and compressed in PHA space, so-called **BRIGHT2** data. In cases where the majority of the data were taken in **FAINT** mode, we adopted the **BRIGHT2** data. Otherwise we combined the **FAINT** mode data with the **BRIGHT** mode, to maximize the signal-to-noise ratio. The data modes we used are listed in column 4 of Table 2. In the case of mixed clocking modes, we chose only that mode with the highest exposure time. This is tabulated in column 5 of Table 2. The exception to this is MCG-2-58-22, where we used the 2-CCD mode data, as even though the exposure time in 4-CCD mode was marginally greater, 2-CCD mode is better calibrated. We excluded periods where telemetry saturation caused severe data dropouts. These usually occurred with 4-CCD mode data in **LOW** bit-rate and such data were generally avoided, although in one case saturation occurred in 1-CCD mode and another in **MEDIUM** bit-rate. Otherwise, we combined the **LOW**, **MEDIUM** and **HIGH** bit-rate data.

We applied data selection and cleaning algorithms using the `ascascreen` script supplied with the `FTOOLS/XSELECT` package version 3.4. Table 3 shows the selection

criteria which were applied to the datasets, unless otherwise noted in Table 2. Flexible criteria (such as `BR_EARTH`, `ELV` and `ANG_DIST`) were determined from an examination of the housekeeping data. For the SIS, the constraints on `BR_EARTH` and `ELV` were determined from an inspection of the SIS event rates (for the on-source chip: SIS0 chip 1 or SIS1 chip 3) as a function of these parameters. A marked increase in the event rate is observed below the angle where significant contamination occurs. In cases where the attitude (`ANG_DIST`) varied wildly (by $\gg 1$ arcmin) during the majority of the observation, that observation was rejected. In two observations, the attitude was relatively stable, but the angle between the source and pointing position often exceeded the default criterion of `ANG_DIST`<0.01 used by `ascascreen` resulting in unacceptable data loss. In these cases we allowed `ANG_DIST`<0.02. Finally, we applied the standard algorithm to remove “hot” and “flickering” pixels from the SIS data.

The exposure times for the screened events files are listed in column 6 of Table 2. We have excluded observations where the exposure in either SIS was less than 10ks to ensure a similar baseline for timing analysis and sufficient signal-to-noise ratio for spectral analysis. Details of the spectral analysis are presented in Nandra et al. 1996b (hereafter paper II) and George et al. 1996 (hereafter paper III). This left 23 observations suitable for further analysis.

4. Spatial analysis

After extracting the event files we accumulated and examined the images for each instrument. The source centroids were generally within ~ 1 arcmin of the optical position of the Galaxy (Fig. 2), which is consistent with the positional uncertainty due to attitude reconstruction errors (Gotthelf, priv. comm.). Mrk 335 and NGC 4051 have larger offsets (~ 1.5 arcmin). Nonetheless, in both cases we are confident that the AGN are the sources of the X-rays observed by *ASCA*, as the *ROSAT* PSPC positions, which are more accurate than those derived from the SIS, are consistent with the optical nuclei, and show no other bright sources within the SIS point-spread function (PSF).

We did not find any evidence for extended emission, although this is not surprising considering the width of the PSF. Even at the distance of the closest galaxy, the half-power diameter (HPD) corresponds to a distance of ~ 5 kpc, much larger than the expected size of the nuclear X-ray source. Visual inspection of the SIS and GIS images revealed six fields with evidence for sources other than the target. These are listed in Table 4. In all cases these were much weaker than the Seyfert and did not cause any serious problems in analysis. Other, even weaker sources may be present in the images, but the presence of

the central target, which is in general very bright, makes the application of point-source searching algorithms difficult. We have not therefore attempted any more sophisticated spatial analysis, but naturally, we avoided the visible contaminating sources when choosing source and background regions.

Due to small calibration differences between the SIS chips, we restricted our analysis to the primary on-source chip for each SIS (SIS0 chip 1 and SIS1 chip 3). In most cases we used a circular extraction cell for the source region, typically 3 – 4 arcmin in radius. However, in cases where the source centroid was close to the gap between SIS chips, a circular extraction cell resulted in an unacceptable loss of counts. In these cases we employed rectangular extraction cells of a similar area. Background for the SIS was estimated using polygonal regions at the edge of the same chip. For the GIS, the analysis was generally simpler and in all cases we adopted a circular source region centered on the AGN. Background counts were taken from source-free regions.

5. Timing analysis

Initially, light curves of the source region were constructed for each observation using the XRONOS package. To increase the signal-to-noise ratio, we combined the SIS0 and SIS1 detectors when analyzing the SIS data; we also combined GIS2 with GIS3. In order to maximize the light curve data thus obtained, we initially accumulated a light curve in 128s bins, requiring all such bins to be fully exposed in both instruments (SIS0/SIS1 or GIS2/GIS3). This ensured that sufficient counts were obtained in each 128s integration for Gaussian statistics to be appropriate, even when the light curves were split into different energy ranges (see below). We were then able to test for variability by means of a χ^2 test against the hypothesis that the flux was constant. The reduced- χ^2 values, χ^2_ν , are quoted in Table 5 for four light curves: SIS0+SIS1 full band (0.5-10 keV; column 2), GIS2+GIS3 hard band (2-10 keV; column 3), SIS0+SIS1 hard band (2-10 keV; column 4) and SIS0+SIS1 soft band (0.5-2.0 keV; column 5). We excluded NGC6814 from this analysis, which was too weak to search for variations on these short timescales. For the remaining sources, variations in the background have a negligible effect on our analysis. We estimate that variability of the SIS background would contribute less than 10^{-4} to the σ_{RMS}^2 values quoted in Table 6 and hence a negligible effect on the χ^2 values quoted in Table 5.

For the SIS full-band light curve (column 2), 15 of the 17 objects tested showed short-timescale variability at > 99 per cent confidence. The exceptions to this are Fairall-9, which showed variability at > 95 per cent confidence and MCG-2-58-22, which showed no significant changes. In almost all cases this variability is confirmed in the GIS and in the

hard and soft bands of the SIS. We conclude that short-timescale variability is extremely common in Seyfert 1 galaxies, albeit at low amplitude in some cases.

The full-band SIS light curves are shown in Fig. 3, and demonstrate a rich diversity of variability characteristics. For example, the individual sources exhibit different amplitudes of variability. To quantify this further, we have calculated the normalized “excess variance”, σ_{RMS}^2 of each light curve. We designate the count rates for the N points in each light curve as X_i , with errors σ_i . We further define μ as the unweighted, arithmetic mean of the X_i . Then:

$$\sigma_{\text{RMS}}^2 = \frac{1}{N\mu^2} \sum_{i=1}^N [(X_i - \mu)^2 - \sigma_i^2]$$

The error on σ_{RMS}^2 , asymptotically for large N , is given by $s_D/(\mu^2\sqrt{N})$ (M.G. Akritas, priv. comm) where:

$$s_D^2 = \frac{1}{N-1} \sum_{i=1}^N [(X_i - \mu)^2 - \sigma_i^2] - \sigma_{\text{RMS}}^2\mu^2$$

i.e. the variance of the quantity $(X_i - \mu)^2 - \sigma_i^2$. These values are given in Table 6. As noted by Lawrence & Papadakis (1993) this parameter depends on the observation length. A more rigorous approach would be to define the amplitude and slope of the PDS. Unfortunately, however, such an analysis is extremely difficult with unevenly sampled data, as afforded by low-earth satellites such as *ASCA*. We justify our use of σ_{RMS}^2 as a measure of the variability power by noting that the σ_{RMS}^2 is correlated with the power-spectrum normalization in the *EXOSAT* data (Lawrence & Papadakis 1993) and that our observations are not radically different in duration (Table 6). There are clear differences between the sources. Furthermore, as shown in Fig. 4, σ_{RMS} shows a strong anti correlation with X-ray luminosity, confirming the previous results (see Section 6). Note that the duration of the observation, t_D , is not correlated with luminosity. We find $\sigma_{\text{RMS}}^2 \propto L_X^{-0.71 \pm 0.03}$, but with a substantial scatter, particularly for the objects around $L_X \sim 10^{43}$ erg s⁻¹. We note with interest, and discuss later, the fact that NGC 4151 shows evidence for changes in σ_{RMS}^2 at different epochs.

We have also employed the energy resolution of the SIS detectors to compare σ_{RMS}^2 for two separate energy bands. We compare the hard band (2-10 keV) and soft band (0.5-2.0 keV) variability in Fig. 5. There is clearly a strong correlation. However, we find that the amplitude of variability in the soft band is often greater than in the hard band. This implies spectral variability for these sources.

In Table 7 we show tests against the constant hypothesis for light curves in 5760s bins (approx 1 orbit) for all our observations. The sources show even stronger evidence for variability on these \sim hr timescales, in all instruments and energy ranges. We were also able to test for variability in NGC 6814 on this timescale, but no evidence for significant flux changes was found. The σ_{RMS}^2 values are not quoted for these light curves as there are generally insufficient points to make the error bars meaningful.

5.1. High-frequency variability

The high signal-to-noise ratio of our *ASCA* data allows us, in principle, to explore the PDS in a regime not accessible to *EXOSAT*. Above a frequency of $\sim 10^{-3}$ Hz, the latter data were dominated by Poisson noise. The low background rate of the *ASCA* detectors should allow us to go beyond this point, into the regime where we might expect cutoffs due to the fundamental size-scale of the X-ray source. However, the uneven sampling prevents construction of a reliable periodogram from our data. Indeed, as noted before, even the σ_{RMS}^2 values quoted above are susceptible to scatter due to the sampling patterns. We have tested for the presence of very rapid variability using light curves of the source accumulated in 32s bins, in the SIS full band. Even for the weakest sources, each bin contains ~ 20 counts, allowing Gaussian statistics to be applied (although once again, we excluded NGC 6814 from the analysis). We searched for contiguous segments with 5 or more bins in each 32s light curve, and performed a χ^2 test against a constant hypothesis for each segment, flagging each time the probability of obtaining that χ^2 by chance was < 1 per cent. The results are shown in Table 8. We find at least one “variable” segment (at > 99 per cent confidence) in 10/23 observations and 9/17 of the sources. However, given that there are typically several tens of segments tested for each observation, the chance of spurious detections is fairly high. We consider there to be firm evidence for ultra-rapid variability if two or more segments show an unacceptable χ^2 , which is true in 5/17 sources. Unsurprisingly, these tend to be the sources with the largest overall variability amplitudes.

For those sources with significant variability on these short time scales, we also tested the hypothesis that the high-frequency PDS was constant in shape and intensity. We achieved this by calculating the excess variance for contiguous segments constructed to have the same duration. If the process producing the variability were statistically stationary, we would then expect these σ_{RMS}^2 values to be constant. Given that our prescription for the error bars on the excess variance is only valid in the limit of large N , we used only segments with > 30 points. This requirement meant that we could not test the constancy hypothesis in NGC 4051 and NGC 3227, since there were no such segments in the SIS light

curve. The χ^2 values and the probabilities of obtaining them are given in columns 5 and 6 of Table 8. In two cases, Mrk 766 and MCG-6-30-15(2), we find an unacceptable χ^2 value, indicating that the high frequency PDS in these sources is variable. Although intriguing, we consider this result to be somewhat tentative, particularly in the case of Mrk 766; some of the excess χ^2 in that source comes from σ_{RMS}^2 values which are less than zero. Whilst these are expected by chance, they may be exaggerating the significance in this case.

6. Discussion

We have presented *ASCA* imaging and timing data for a sample of Seyfert 1 galaxies, most of which were originally detected by large-beam X-ray instrumentation. The *ASCA* images demonstrate that, aside from the now infamous case of NGC 6814, and despite the lack of spatial resolution of those instruments, the Seyfert galaxies identified in the Ariel-V and *HEAO-1* surveys are indeed the sources of hard X-ray emission. There are weak contaminating sources in some cases, but none which have a measurable impact on our current analysis, or seem likely to have contaminated previous observations significantly.

Our sources show variability to be very common, albeit at very low amplitudes for some objects. This emphasizes the need for high signal-to-noise ratio observations; this low-level variability was missed with most previous instrumentation. The RMS variability amplitude is strongly anti-correlated with the X-ray luminosity of the source, but there is a substantial scatter. Some of this could be due to the fact that the observation durations differ, although we note that the *EXOSAT* data also showed a significant spread of power-spectrum normalizations about the correlation. Were the sampling and power spectra identical for all sources then σ_{RMS}^2 should be proportional to the amplitude of the PDS at a given frequency. Therefore we compare our correlation index of 0.71 with that given by Green et al. of 0.68 and Lawrence & Papadakis of 0.55. The fact that these agree well, despite the expected deviations due to the sampling patterns, supports the result that the shapes of the power spectra are at least very similar from source to source, and that the effects of the observation duration are not severe.

It is currently unclear whether the X-ray source in Seyfert galaxies consists of a single, coherent region or of multiple “hot spots”, although the lack of any obvious characteristic time scale would tend to favor the latter (e.g., McHardy & Czerny 1987). In such a scenario, one could explain an anti-correlation of σ_{RMS}^2 with L_X by hypothesizing that the higher luminosity sources simply contained more hot spots, such that the large amplitude variability was “washed out”. We would then expect $\sigma_{\text{RMS}}^2 \propto L_X^{-1}$, which is somewhat steeper than the observed correlation, although we note that the scatter evident in Fig. 4

makes precise determination of the relation difficult. Nonetheless, our results, and those derived from the *EXOSAT* data, would tend to argue that the individual shots carried more power in the higher-luminosity sources, rather than simply being more numerous. Alternatively, with a single X-ray-producing region, one might hypothesize that the luminosity is related to the size of that region. For example, if the source size is a fixed number of gravitational radii, we expect it to be proportional to the mass of the black hole. With a fixed accretion rate (with respect to the Eddington limit), \dot{M} , we would once again expect $\sigma_{\text{RMS}}^2 \propto L_{\text{X}}^{-1}$. Our observed correlation would suggest that \dot{M} increases with L , a view supported by some recent *ROSAT* and *ASCA* spectral data for quasars (Stewart et al. 1995; Nandra et al. 1996a).

The soft X-ray emission in our sources generally shows a larger amplitude of variability than the hard X-rays on the time scales considered. In this case the sampling is identical for the hard and soft X-ray light curves, so that if the power spectra were identical in the two bands, we would not expect significant differences in σ_{RMS}^2 . To date, the power spectra in the soft X-ray band (e.g., the *EXOSAT* LE) are not well known. For two sources with well-defined LE power spectra, NGC 4051 and MCG-6-30-15 (which are also in our sample), it appears that the power spectra are different in the soft and hard X-ray bands (Green et al. 1993; Papadakis & Lawrence 1995). For those sources the power spectra appear to be steeper in the soft X-ray band, although we note that in both cases there have been claims of quasi-periodic oscillations in the power spectra (Papadakis & Lawrence 1993; Papadakis & Lawrence 1995), making the spectral slope of the PDS much more difficult to define. It is difficult to compare our result with theirs, as our σ_{RMS}^2 represents an integration of the power spectrum over some frequency range, and cannot be easily equated to the slope. We note, however, that, even in the soft X-ray band, the energy spectrum is probably dominated by the power law component (see paper III). Therefore, we would anticipate the variability characteristics in the two bands to be similar. However, additional spectral complexity – and spectral variability – in the soft X-ray band could lead to additional variance. For example, changes in the ionization parameter or column density of a warm absorber (e.g. Halpern 1984; Pan, Stewart & Pounds 1990) would have most effect in the soft X-ray band, as would any independently-variable soft excess (e.g. Turner & Pounds 1988; such excesses are also clearly evident in a number of these spectra – see Paper III).

We find evidence that NGC 4151 shows changes in σ_{RMS}^2 in apparent contradiction to the suggestion that the process producing the variability is statistically stationary (Green et al. 1993; Papadakis & Lawrence 1995). Lawrence & Papadakis (1993) also found changes in σ_{RMS}^2 between observations of NGC 4151, but as they showed, the power spectra for those observations are consistent. Indeed, we find here that the longest observation of NGC 4151(2) has the highest variance, which we expect as we are sampling the longer

time scales. Interestingly, however, a comparison of observations (4) and (5) show the latter to have a higher variance, despite a shorter duration. This suggests that the shape and/or normalization of the power spectrum changes at different epochs. The other sources with multiple observations do not show clear evidence for variations in σ_{RMS}^2 , when the observation durations are taken into account.

We found evidence for variability power on frequencies higher than $\sim 10^{-3}$ Hz for five sources. In two cases there is also a suggestion that the variability amplitude changes during the observation. This indicates that the high-frequency PDS in these sources is not constant. A variable PDS might imply changes in fundamental time scales in the source. At the high frequency end, this might be related to the size-scale of the X-ray producing region(s). Our observations suggest that it might be fruitful to pursue the study of the PDS in the $10^{-3} - 10^{-2}$ Hz range with future instrumentation.

We are grateful to Eric Gotthelf for his help in determining the source positions and information regarding the positional accuracy of the *ASCA* data, Lorella Angelini for many helpful discussions, the *ASCA* team for their operation of the satellite, the *ASCA* GOF at NASA/GSFC for their assistance in data analysis, and Michael Akritas of the SCCA operated at the Department of Statistics, Penn State University for discussions and information on statistical matters. This research has made use of the Simbad database, operated at CDS, Strasbourg, France; of the NASA/IPAC Extragalactic database, which is operated by the Jet Propulsion Laboratory, Caltech, under contract with NASA; and data obtained through the HEASARC on-line service, provided by NASA/GSFC. We acknowledge the financial support of the National Research Council (KN) and Universities Space Research Association (IMG, TJT, TY).

Table 1. The *ASCA* Seyfert 1 sample.

Name	Alt. Name	RA (J2000)	DEC (J2000)	z (V93)	Class	$N_{\mathrm{H}}(\mathrm{Gal})^a$
Mrk 335	PG	00 06 19.4	20 12 11	0.025	1.0 (W92)	4.0
Fairall 9	...	01 23 45.7	-58 48 21	0.046	1.0 (W92)	3.0
3C 120	Mrk 1506	04 33 11.0	05 21 15	0.033	1.0 (G95)	12.3
NGC 3227	...	10 23 30.5	19 51 55	0.003	1.5 (O93)	2.2
NGC 3516	...	11 06 47.4	72 34 06	0.009	1.5 (O93)	2.9
NGC 3783	...	11 39 01.7	-37 44 18	0.009	1.2 (W92)	8.9
NGC 4051	...	12 03 09.5	44 31 52	0.002	1.0 (O95)	1.3
NGC 4151	...	12 10 32.4	39 24 20	0.003	1.5 (O95)	2.1
Mrk 766	NGC 4253	12 18 26.6	29 48 46	0.012	1.5 (W92)	1.6
NGC 4593	Mrk 1330	12 39 39.3	-05 20 39	0.009	1.0 (W92)	2.0
MCG-6-30-15	...	13 35 53.3	-34 17 48	0.008	1.0 (G95)	4.1
IC 4329A	...	13 49 19.2	-30 18 34	0.016	1.0 (W92)	10.4
NGC 5548	Mrk 1509	14 17 59.5	25 08 12	0.017	1.5 (O95)	1.7
Mrk 841	PG	15 04 01.1	10 26 16	0.036	1.5 (O95)	2.2
NGC 6814	...	19 42 40.5	-10 19 24	0.006	1.2 (W92)	9.8
Mrk 509	...	20 44 09.6	-10 43 23	0.035	1.2 (W92)	4.2
NGC 7469	Mrk 1514	23 03 15.5	08 52 26	0.017	1.0 (O95)	4.8
MCG-2-58-22	Mrk 926	23 04 43.4	-08 41 08	0.047	1.2 (W92)	3.4

^aGalactic HI column density from 21cm measurements in units of $10^{20} \mathrm{cm}^{-2}$

References. — V93: Veron-Cetty & Veron (1993). G95: Giuricin, Mardirossian & Mezzetti (1995); O93: Osterbrock & Martel (1993); W92: Whittle (1992). N_{H} values are from Elvis, Lockman & Wilkes (1989); Stark et al. (1992) or the HEASARC online service.

Table 2. *ASCA* observation log.

Name	Seq.	Date	CCD mode	t_{exp}	Count rate	Ref
Mrk 335 ^a	71010000	93.343	BRIGHT (2)	19.3	0.584 ± 0.006	
Fairall 9	71027000	93.325	FAINT (1)	22.0	1.003 ± 0.007	
3C 120 ^{a,f}	71014000	94.048	FAINT (1)	47.4	1.871 ± 0.006	
NGC 3227	70013000	93.128	BRIGHT (4)	33.4	0.665 ± 0.005	P94
NGC 3516 ^{b,f}	71007000	94.092	FAINT (1)	33.7	2.500 ± 0.010	
NGC 3783(1)	71041000	93.353	BRIGHT (1)	17.5	1.067 ± 0.008	G95
NGC 3783(2)	71041010	93.357	BRIGHT (2)	14.9	1.324 ± 0.010	G95
NGC 4051 ^a	70001000	93.115	BRIGHT (4)	27.6	1.063 ± 0.006	M94
NGC 4151(1) ^{b,e}	70000000	93.144	BRIGHT (4)	W94
NGC 4151(2) ^a	70000010	93.309	FAINT (1)	13.4	2.149 ± 0.013	W94
NGC 4151(3) ^d	71019030	93.338	BRIGHT (2)	Y95
NGC 4151(4)	71019020	93.339	FAINT (2)	10.8	2.190 ± 0.015	Y95
NGC 4151(5)	71019010	93.341	BRIGHT (2)	11.7	2.479 ± 0.015	Y95
NGC 4151(6) ^e	71019000	93.343	FAINT (2)	Y95
Mrk 766 ^a	71046000	93.352	FAINT (1)	33.7	0.903 ± 0.006	
NGC 4593 ^{b,f}	71024000	94.009	FAINT (1)	23.1	1.567 ± 0.009	
MCG-6-30-15(1)	70016000	93.190	BRIGHT (2)	29.8	1.961 ± 0.009	F94
MCG-6-30-15(2) ^a	70016010	93.212	BRIGHT (1)	31.4	1.290 ± 0.007	F94
IC 4329A ^{a,b}	70005000	93.227	BRIGHT (4)	29.1	2.096 ± 0.009	M95
NGC 5548 ^{b,c}	70018000	93.208	BRIGHT (4)	20.4	1.933 ± 0.010	M95
Mrk 841(1) ^g	70009000	93.234	BRIGHT (2)	30.5	0.477 ± 0.004	G96

Table 2—Continued

Name	Seq.	Date	CCD mode	t_{exp}	Count rate	Ref
Mrk 841(2) ^f	71040000	94.052	BRIGHT (2)	20.9	0.355 ± 0.004	G96
NGC 6814(1)	70012000	93.124	BRIGHT (4)	40.3	0.029 ± 0.001	
NGC 6814(2) ^d	70012010	93.304	BRIGHT (4)	
NGC 6814(3) ^d	70012020	93.305	BRIGHT (4)	
Mrk 509	71013000	94.119	FAINT (1)	40.1	2.120 ± 0.008	G94
NGC 7469(1) ^e	71028000	93.328	FAINT (2)	
NGC 7469(2) ^g	71028030	93.330	FAINT (2)	14.5	1.175 ± 0.009	
NGC 7469(3) ^e	71028010	93.336	FAINT (2)	
MCG-2-58-22 ^c	70004000	93.145	FAINT (2)	13.3	0.444 ± 0.006	W95

^aELV>5

^bSome data excluded due to saturation

^cBR_EARTH>25 (SIS0)

^dObservation rejected due to bad attitude

^eObservation rejected due to low exposure

^fAffected by GIS3 BITFIX problem

^gANG_DIST<0.02

References. — F94: Fabian et al. 1994; G94: Guinazzi et al. 1994; G95: George, Turner & Netzer 1995; M94: Mihara et al. 1994; M95: Mushotzky et al. 1995; P94: Ptak et al. 1994; W94: Weaver et al. 1994; W95: Weaver et al. 1995; Y95: Yaqoob et al. 1995

Note. — Column 1: Name and number of observation; Column 2: *ASCA* processing sequence number; Column 3: Date of observations (year.day); Column 4: SIS data mode and clocking mode; Column 5: Screened exposure time in SIS0 (ks); Column 6: Count rate in SIS0 (ct s⁻¹); Column 7: reference for previously-published *ASCA* data

Table 3. Selection criteria

Criterion	Description
All instruments	
SAA = 0	Satellite outside South Atlantic Anomaly
ANG_DIST < 0.01	Angular offset from nominal pointing position (°)
RBM_CONT < 500	Radiation Belt Monitor
COR > 6	Cut-off rigidity (GeV/c)
SIS only	
ELV > 10	Angle from earth's limb (°)
BR_EARTH > 20	Angle from bright earth (°)
T_DY_NT > 50, 100, 200 ^a	Time after day/night terminator (s)
Sx_PIXLy ^b < 50, 75, 100 ^a	SIS pixel threshold
GIS only	
ELV > 5	Angle from earth's limb (°)

^aFor 1,2,4 CCD modes respectively

^bx=SIS number; y=chip number

Table 4. Serendipitous sources

Field	RA	DEC	Count Rate	ID	Class	Det
NGC 3516	11 02 31	72 46 37	0.021 ± 0.002	MS 10590+7302	QSO	GIS
NGC 4151	12 10 25	39 29 24	0.237 ± 0.005	1207+39W4	BL Lac	SIS
Mrk 766	12 18 54	29 57 57	0.008 ± 0.001	GIS
NGC 4593	12 40 27	-05 13 59	0.010 ± 0.001	1WGA J1240.4-0514	...	GIS
NGC 5548	14 18 30	25 10 38	0.076 ± 0.003	1E1416.2+2525	Cluster	SIS
Mrk 841	15 03 40	10 16 49	0.015 ± 0.001	GIS ^a
Mrk 841	15 04 24	10 29 36	0.007 ± 0.001	PKS 1502+106	HPQ	GIS

^aVariable source

Note. — Column 1: Primary target; Column 2: Right ascension of X-ray position of serendipitous source (J2000); Column 3: Declination (J2000); Column 4: Source identification; Column 5: Instrument where detected

Table 5. $\chi^2_v/\text{d.o.f.}$ for 128s light curves

Name	SIS full 0.5-10 keV	GIS hard 2-10 keV	SIS soft 0.5-2 keV	SIS hard 2-10 keV
Mrk 335	1.67/106	1.25/134	1.45/106	1.21/106
Fairall 9	1.23/140	1.07/245	1.12/140	1.08/140
3C 120	2.52/259	1.25/280	2.14/259	1.42/259
NGC 3227	9.14/93	4.06/272	7.71/93	2.94/93
NGC 3516	5.20/183	2.85/267	4.28/183	1.90/183
NGC 3783(1)	3.50/89	2.02/155	2.16/89	2.36/89
NGC 3783(2)	2.71/83	1.97/121	1.87/83	1.85/83
NGC 4051	20.7/83	7.07/184	17.5/83	4.50/83
NGC 4151(2)	10.7/62	... ^a	3.64/62	8.26/62
NGC 4151(4)	2.81/52	3.00/75	1.49/52	2.45/52
NGC 4151(5)	4.69/64	4.65/92	1.52/64	13.84/64
Mrk 766	19.6/195	4.37/226	17.2/195	4.31/195
NGC 4593	8.01/136	2.76/239	6.74/136	2.47/136
MCG-6-30-15(1)	22.4/163	13.4/218	16.9/162	6.30/162
MCG-6-30-15(2)	16.4/176	5.37/215	12.3/176	5.40/176
IC 4329A	2.23/52	1.36/238	1.60/52	1.74/52
NGC 5548	3.40/19	1.47/208	3.17/19	1.22/19
Mrk 841(1)	1.67/184	1.20/235	1.48/184	1.14/184
Mrk 841(2)	1.40/95	1.05/123	1.34/95	1.18/95
NGC 6814(1) ^b
Mrk 509	1.40/243	0.98/121	1.34/243	1.17/243
NGC 7469(2)	2.38/86	1.30/136	1.95/86	1.42/86
MCG-2-58-22	1.19/56	1.05/221	1.25/56	0.90/56

^aGIS exposure too low for meaningful analysis

^bSource too weak for analysis on this timescale

Table 6. Variability amplitude ($10^{-2}\sigma_{\text{RMS}}^2$) for 128s light curves

Name	SIS full 0.5-10 keV	GIS hard 2-10 keV	SIS soft 0.5-2 keV	SIS hard 2-10 keV	t_{D}^a (ks)
Mrk 335	0.47 ± 0.15	0.50 ± 0.31	0.42 ± 0.16	0.74 ± 0.46	50.7
Fairall 9	0.09 ± 0.06	0.11 ± 0.15	0.06 ± 0.07	0.07 ± 0.20	56.7
3C 120	0.38 ± 0.06	0.17 ± 0.08	0.40 ± 0.07	0.35 ± 0.10	131.0
NGC 3227	5.80 ± 0.90	2.80 ± 0.30	8.40 ± 1.40	3.00 ± 0.60	85.8
NGC 3516	0.71 ± 0.09	0.76 ± 0.08	0.86 ± 0.12	0.44 ± 0.09	79.5
NGC 3783(1)	0.93 ± 0.19	0.73 ± 0.16	0.91 ± 0.24	0.92 ± 0.23	38.3
NGC 3783(2)	0.53 ± 0.11	0.64 ± 0.17	0.55 ± 0.18	0.48 ± 0.16	37.5
NGC 4051	12.0 ± 1.70	5.80 ± 0.74	13.1 ± 2.00	9.00 ± 1.50	84.2
NGC 4151(2)	2.60 ± 0.80	... ^b	3.00 ± 1.00	2.50 ± 0.80	50.9
NGC 4151(4)	0.32 ± 0.10	0.41 ± 0.08	0.55 ± 0.31	0.30 ± 0.11	29.1
NGC 4151(5)	0.62 ± 0.10	0.67 ± 0.09	0.37 ± 0.24	0.58 ± 0.09	25.9
Mrk 766	7.90 ± 0.60	5.20 ± 0.60	9.50 ± 0.70	5.00 ± 0.50	77.8
NGC 4593	2.10 ± 0.20	2.20 ± 0.30	2.40 ± 0.30	1.40 ± 0.20	96.5
MCG-6-30-15(1)	4.10 ± 0.40	4.40 ± 0.30	4.60 ± 0.40	3.50 ± 0.40	87.9
MCG-6-30-15(2)	5.70 ± 0.70	4.60 ± 0.60	6.40 ± 0.90	4.60 ± 0.70	97.2
IC 4329A	0.24 ± 0.08	0.10 ± 0.03	0.20 ± 0.13	0.35 ± 0.17	85.2
NGC 5548	0.47 ± 0.23	0.23 ± 0.07	0.65 ± 0.28	0.08 ± 0.29	83.3
Mrk 841(1)	0.59 ± 0.14	0.58 ± 0.14	0.58 ± 0.20	0.38 ± 0.36	79.5
Mrk 841(2)	0.35 ± 0.22	-0.11 ± 0.34	0.58 ± 0.37	0.55 ± 0.52	60.9
NGC 6814(1) ^c
Mrk 509	0.08 ± 0.02	-0.02 ± 0.07	0.09 ± 0.03	0.11 ± 0.08	108.0
NGC 7469(2)	0.50 ± 0.14	0.35 ± 0.19	0.50 ± 0.15	0.53 ± 0.32	37.4
MCG-2-58-22	0.14 ± 0.20	0.10 ± 0.22	0.40 ± 0.29	-0.24 ± 0.29	83.3

^aDuration of the observation

^bGIS exposure too low for meaningful analysis

^cSource too weak for analysis on this timescale

Table 7. χ^2_ν /d.o.f for 5760s light curves

Name	SIS full 0.5-10 keV	GIS hard 2-10 keV	SIS soft 0.5-2 keV	SIS hard 2-10 keV
Mrk 335	8.39/7	3.69/7	6.16/7	2.81/7
Fairall 9	2.11/9	0.93/8	1.84/9	1.25/9
3C 120	16.0/22	4.17/22	11.8/22	5.36/22
NGC 3227	42.8/14	53.1/14	37.0/14	10.2/14
NGC 3516	63.1/12	38.6/12	50.9/12	15.5/12
NGC 3783(1)	32.3/6	28.5/6	17.0/6	16.3/6
NGC 3783(2)	30.8/5	22.1/5	16.2/5	14.9/5
NGC 4051	119.6/12	54.8/12	97.7/12	23.8/12
NGC 4151(2)	101.0/6	... ^a	27.1/6	74.4/6
NGC 4151(4)	23.1/4	39.0/4	6.06/4	18.9/4
NGC 4151(5)	57.8/4	83.9/4	11.0/4	46.9/4
Mrk 766	233.7/13	40.3/13	212.3/13	37.1/13
NGC 4593	79.8/11	30.5/14	65.9/11	16.0/11
MCG-6-30-15(1)	188.7/13	139.8/14	143.2/13	47.6/13
MCG-6-30-15(2)	146.8/15	39.2/17	105.3/15	44.5/15
IC 4329A	6.29/12	6.30/14	3.59/12	4.22/12
NGC 5548	4.39/11	5.46/13	4.27/11	1.25/11
Mrk 841(1)	11.8/13	4.16/13	9.55/13	2.99/13
Mrk 841(2)	5.04/10	1.51/10	4.78/10	1.59/10
NGC 6814(1)	0.97/20	0.92/23	1.39/20	0.63/20
Mrk 509	7.45/18	1.92/6	5.38/18	3.43/18
NGC 7469(2)	16.8/6	11.2/6	11.8/6	6.05/6
MCG-2-58-22	1.55/10	1.57/14	1.38/10	1.95/10

^aGIS exposure too low for meaningful analysis

Table 8. Rapid variability; 32s bins

Name	No. of Segments	Longest (s)	Variable Segments	χ^2_ν ^a /d.o.f. (σ^2_{RMS})	$prob^b_{var}$ (σ^2_{RMS})
Mrk 335	25	2112	0
Fairall 9	30	1984	0	0.42/4	0.79
3C 120	69	1632	0	1.25/15	0.22
NGC 3227	55	864	2
NGC 3516	37	1824	2	1.06/12	0.39
NGC 3783(1)	26	1248	1
NGC 3783(2)	18	1312	0
NGC 4051	46	864	2
NGC 4151(2)	22	1152	0
NGC 4151(4)	16	1600	0
NGC 4151(5)	19	1312	0
Mrk 766	37	1760	3	2.99/13	$< 10^{-3}$
NGC 4593	24	1632	0	0.88/9	0.54
MCG-6-30-15(1)	45	1248	5	5.95/5	$< 10^{-4}$
MCG-6-30-15(2)	49	1504	2	0.88/8	0.54
IC 4329A	31	928	0
NGC 5548	19	352	0
Mrk 841(1)	39	2112	1
Mrk 841(2)	33	1120	0
NGC 6814(1)
Mrk 509	62	1632	1	1.05/13	0.40
NGC 7469(2)	19	1536	0	0.70/ 4	0.59
MCG-2-58-22	25	1280	1

^aFor a test of the hypothesis that σ^2_{RMS} was constant. We quote values only for those observations with > 4 segments with > 30 points and used identical sampling for each segment (see text)

^bProbability of obtaining this χ^2 by chance

REFERENCES

- Barr, P., Mushotzky, R.F., 1986, *Nature*, 320, 421
- Elvis, M., Lockman, F. J., Wilkes, B., 1989, *AJ*, 97, 777
- Day, C.S.R., Arnaud, K., Ebisawa, K., Gotthelf, E., Ingham, J., Mukai, K., White, N.E., 1994, *The ABC Guide to ASCA Data Reduction*, NASA/GSFC
- Fabian, A.C., et al., 1994, *PASJ*, 46, 59
- Gendreau, K., 1995, Ph.D. thesis, Massachusetts Institute of Technology
- George, I.M., Turner, T.J., Netzer, H., 1995, *ApJ*, 438, L67
- George, I.M., et al., in preparation (Paper III)
- Giuricin, G., Mardirossian, F., Mezzetti, M., 1995, *ApJ*, 446, 550
- Green, A.R., McHardy, I.M., Lehto, H.J., 1993, *MNRAS*, 265, 664
- Gotthelf, E.V. et al., in preparation
- Halpern, J.P., 1984, *ApJ*, 281, 90
- Lawrence, A., Watson, M.G., Pounds, K.A., Elvis, M., 1985, *MNRAS*, 217, 685
- Lawrence, A., Watson, M.G., Pounds, K.A., Elvis, M., 1987, *Nature*, 325, 694
- Lawrence, A., Papadakis, I.E., 1993, *ApJ*, 41, L93
- McHardy, I.M., Czerny, B., 1987, *Nature*, 325, 696
- Madejski, G.M., Done, C., Turner, T.J., Mushotzky, R.F., Serlemitsos, P., Fiore, F., Sikora, M., Begelman, M.C., 1993, *Nature*, 365, 626
- Marshall, F.E., Holt, S.S., Mushotzky, R.F., Becker, R.H., 1983, *ApJ*, 269, L31
- Marshall, N., Warwick, R.S., Pounds, K.A., 1981, *MNRAS*, 194, 987
- Mihara, T., Matsuoka, M., Mushotzky, R.F., Kunieda, H., Otani, C., Miyamoto, S., Yamauchi, M., 1994, *PASJ*, 46, L137
- Mushotzky, R.F., 1984, *Adv. Space Res.*, 3, 157
- Nandra, K., Pounds, K.A., 1994, *MNRAS*, 268, 405
- Nandra, K., George, I.M., Mushotzky, R.F., Turner, T.J., Yaqoob, T., 1996a, *ApJ*, submitted (Paper II)
- Nandra, K., George, I.M., Turner, T.J., Fukazawa, Y., 1996b, *ApJ*, in press
- Netzer, H., Turner, T.J., George, I.M., 1994, *ApJ*, 435, 106
- Osterbrock, D.E., Martel, A., 1993, *ApJ*, 414, 552

- Otani, C., et al., 1994, in Makino, F., Ohashi, T., Eds, New Horizon of X-ray Astronomy, p655
- Otani, C., Dotani, T., 1994, in ASCA News no. 2
- Pan, H.-C., Stewart, G.C., Pounds, K.A., 1990, MNRAS, 242, 660
- Papadakis, I.E., Lawrence, A., 1993, Nature, 361, 250
- Papadakis, I.E., Lawrence, A., 1995, MNRAS, 272, 161
- Perola, G.C., et al., 1986, ApJ, 306, 508
- Piccinotti, G., Mushotzky, R.F., Boldt, E.A., Holt, S.S., Marshall, F.E., Serlemitsos, P.J., Shafer, R.A., 1982, ApJ, 253, 485
- Pounds, K.A., Turner, T.J, Warwick, R.S., 1986, MNRAS, 221, 7P
- Ptak, A., Yaqoob, T., Serlemitsos, P.J., Mushotzky, R.F., Otani, C., 1994, ApJ, 436, L31
- Stark, A.A., Gammie, C.F., Wilson, R.W., Bally, J., Linke, R.A., Heiles, C., Hurwitz, M., 1992, ApJS, 79, 77
- Stewart, G.C., Georgantopoulos, I., Boyle, B., Shanks, T., Griffiths, R., 1995, in Makino, F., Ohashi, T., Eds, New Horizon of X-ray Astronomy, Universal Academy Press, Tokyo, p331
- Tanaka, Y., Inoue, H., Holt, S.S., 1994, PASJ, 46, L37
- Tennant, A.F., Mushotzky, R.F., 1983, ApJ, 264, 92
- Turner, T.J., 1988, Ph. D. thesis, Leicester University, UK
- Turner, T.J., Pounds, K.A., 1988, MNRAS, 232, 463
- Turner, T.J., Pounds, K.A., 1989, MNRAS, 240, 833
- Turner, M.J.L., et al., 1990, MNRAS, 244, 310
- Veron-Cetty, M.-P, Veron, P., 1993, ESO Sci. Rep., 13, 1
- Weaver, K.A., Yaqoob, T., Holt, S.S., Mushotzky, R.F., Matsuoka, M., Yamauchi, M., 1994, ApJ, 436, 27
- Weaver, K.A., Nousek, J., Yaqoob, T., Hayashida, K., Murakami, S., 1995, ApJ, 451, 147
- Whittle, M., 1992, ApJS, 79, 49
- Yaqoob, T., Warwick, R.S., 1991, MNRAS, 248, 773
- Yaqoob, T., Edelson, R.A., Weaver, K.A., Warwick, R.S., Mushotzky, R.F., Serlemitsos, P.J., Holt, S.S., 1995, ApJ, 453, 81

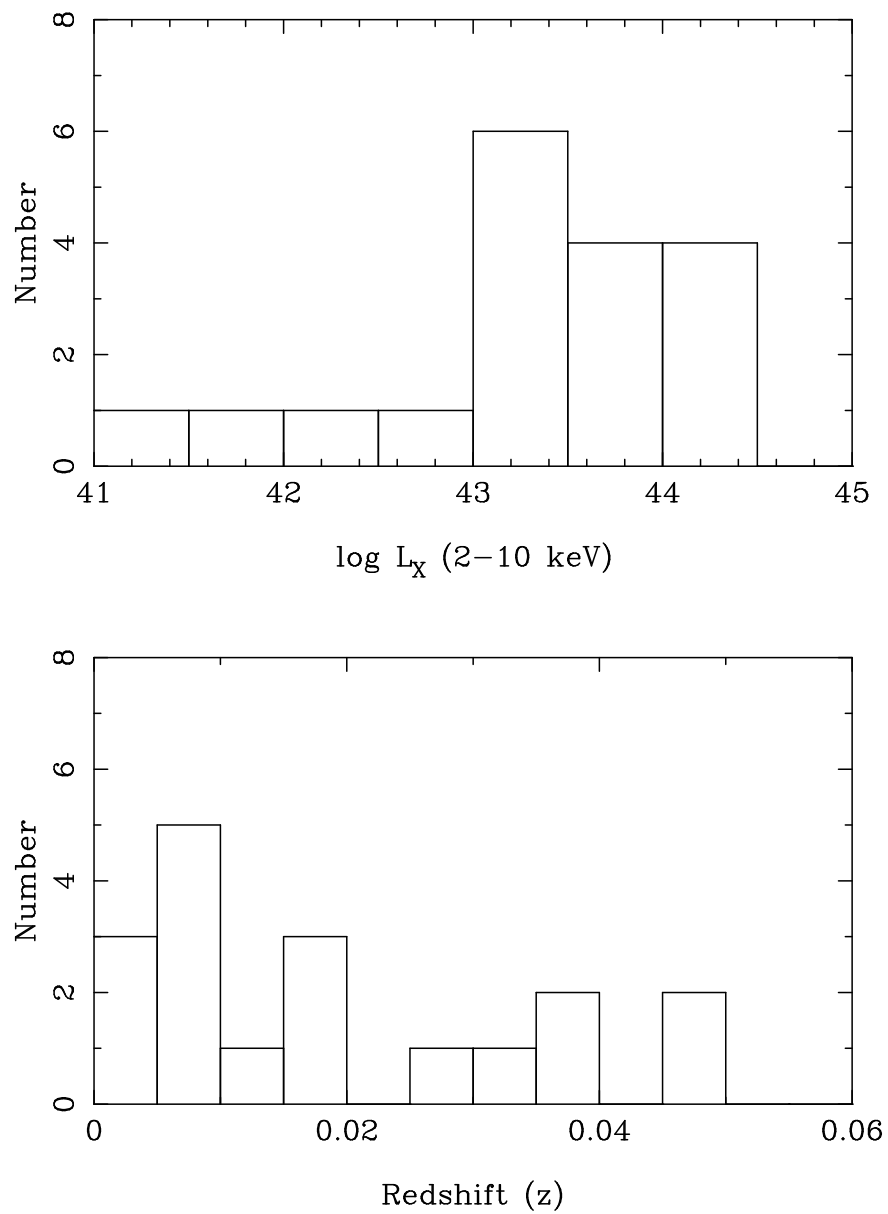


Fig. 1.— Histograms of the X-ray luminosity (upper panel) and redshift (lower panel) for our sample of Seyfert 1 galaxies. The source are chosen to have redshift $z < 0.05$ but cover a wide range of L_X

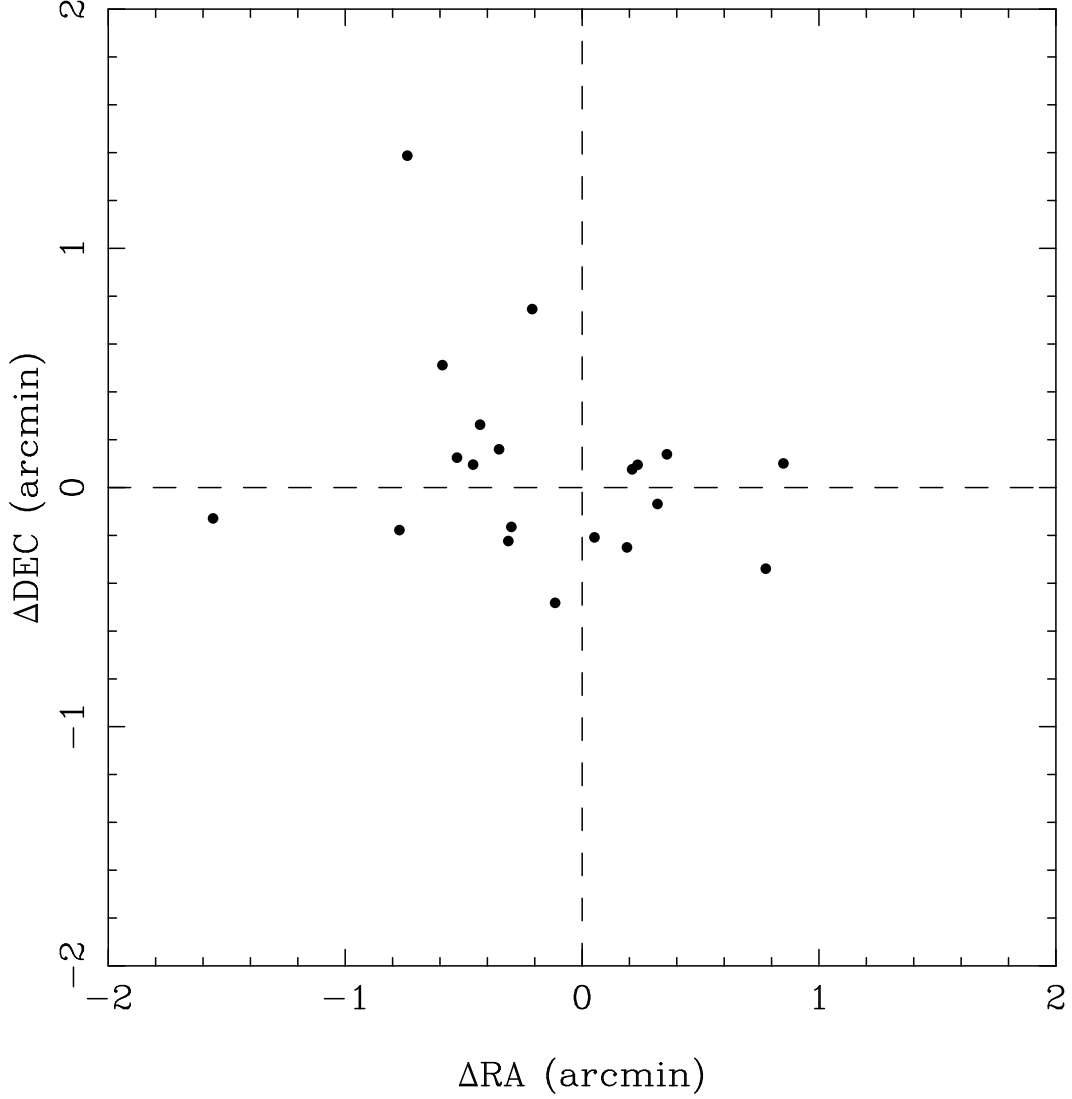
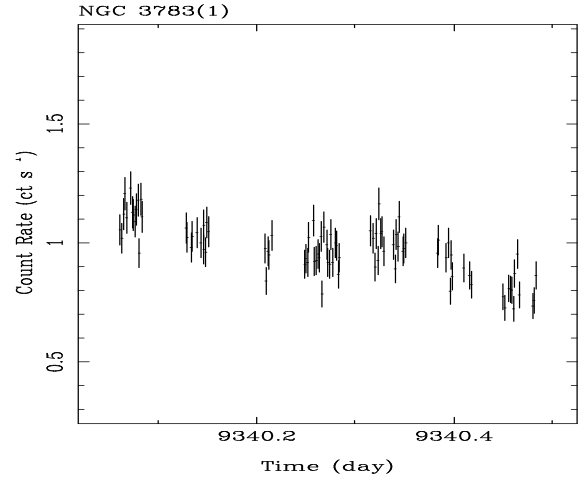
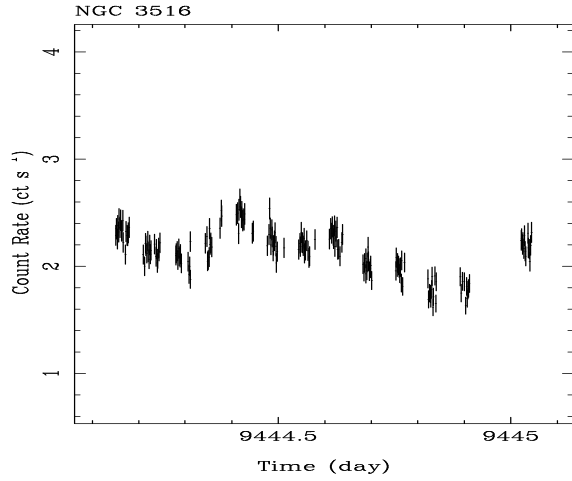
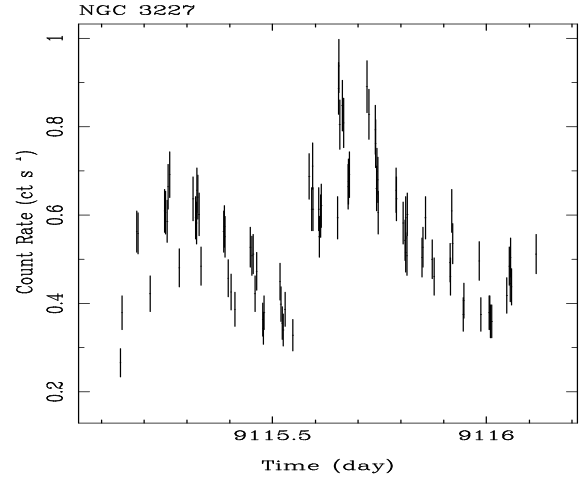
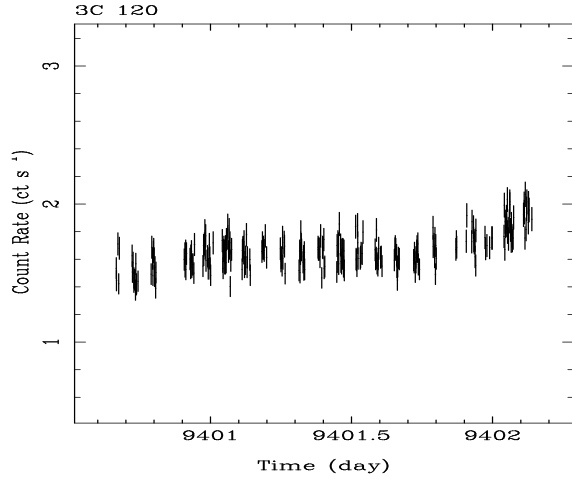
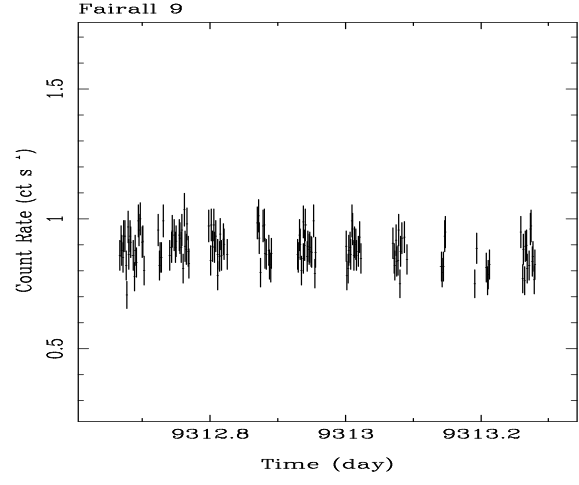
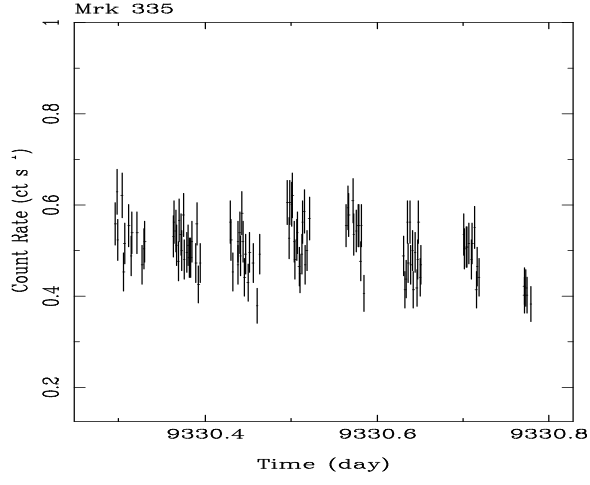
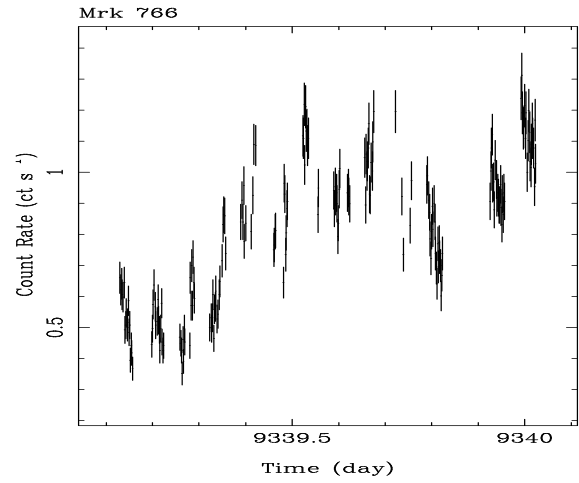
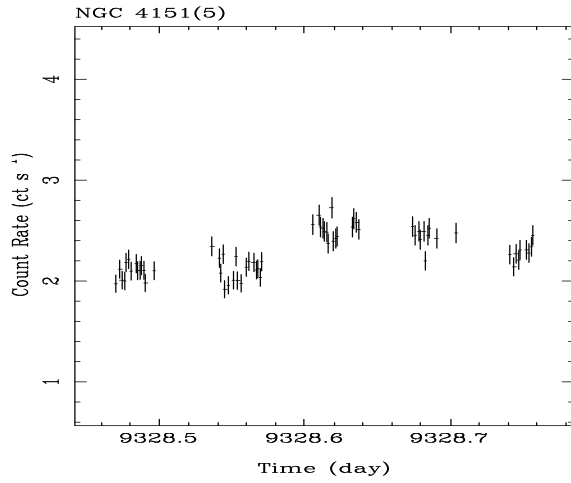
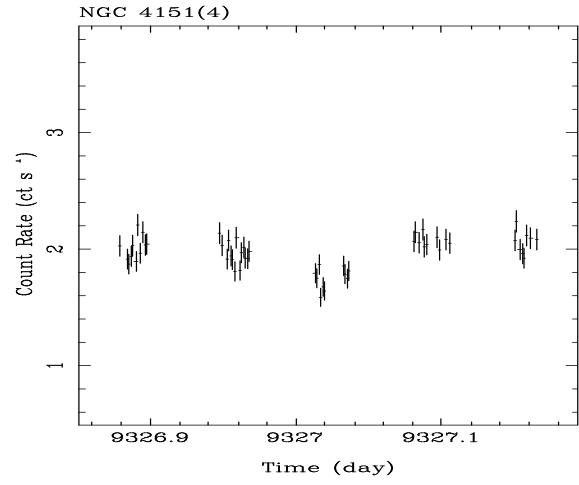
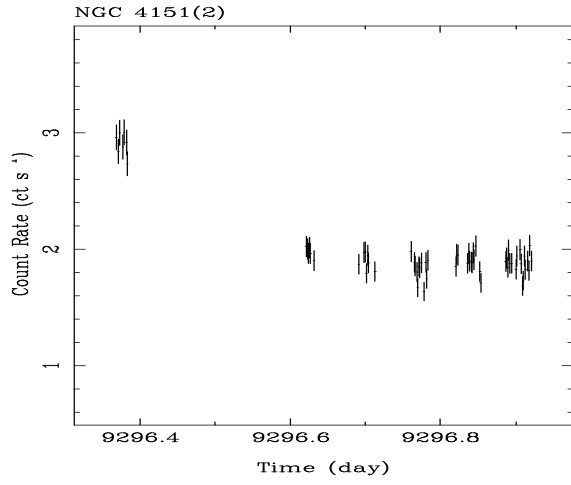
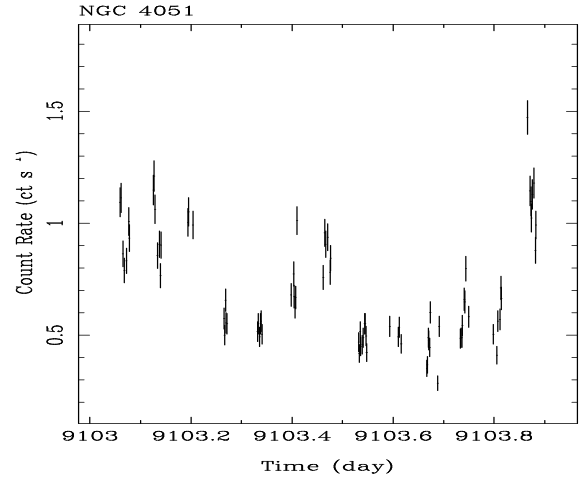
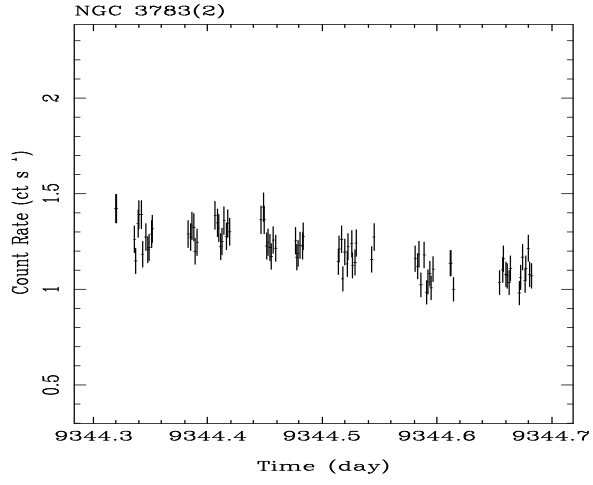
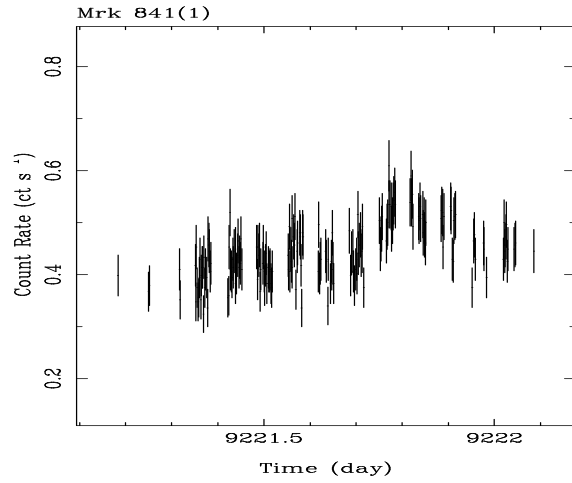
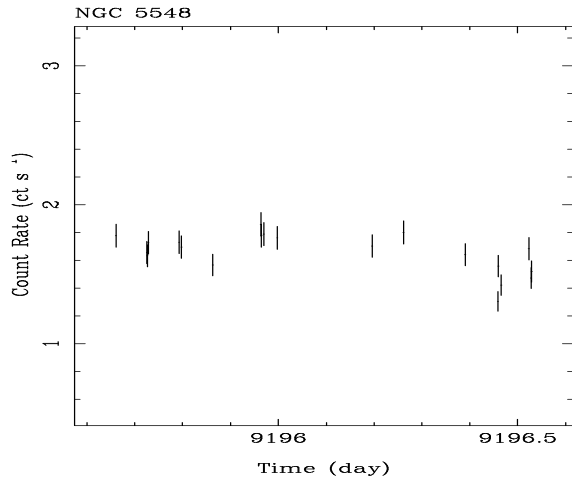
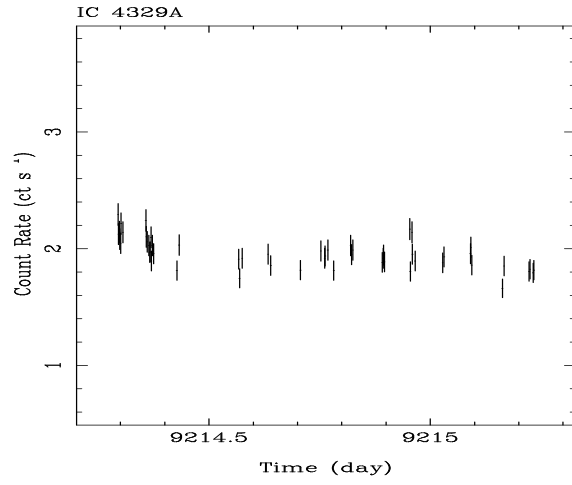
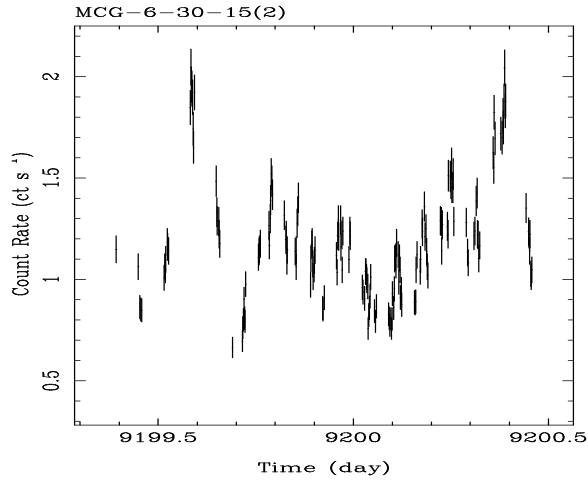
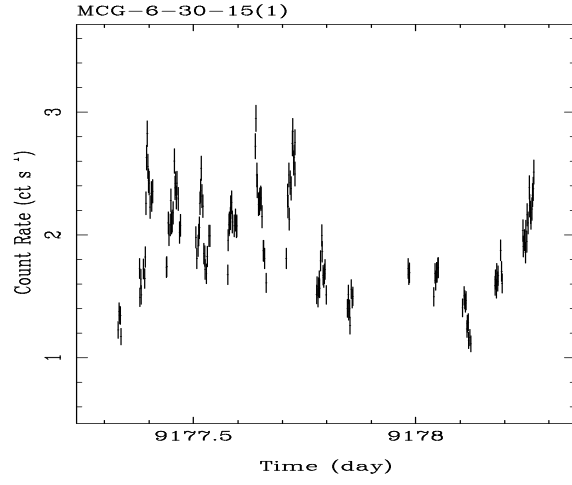
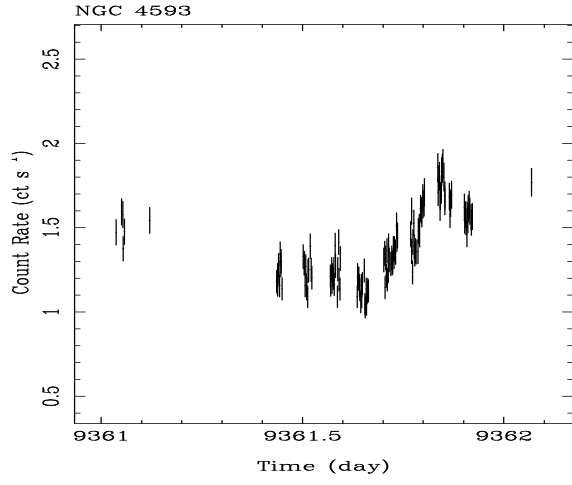


Fig. 2.— Offset of the X-ray and optical position in Right Ascension, versus that in Declination, both in arc minutes. The two positions are generally consistent within the positional accuracy of *ASCA* (~ 0.7 arcmin FWHM; Gotthelf, priv. comm.). Both NGC 4051 and Mrk 335 have unusually large offsets, but we are confident that the AGN is the source of the X-ray emission, as the *ROSAT* PSPC positions agree well with the optical nucleus.







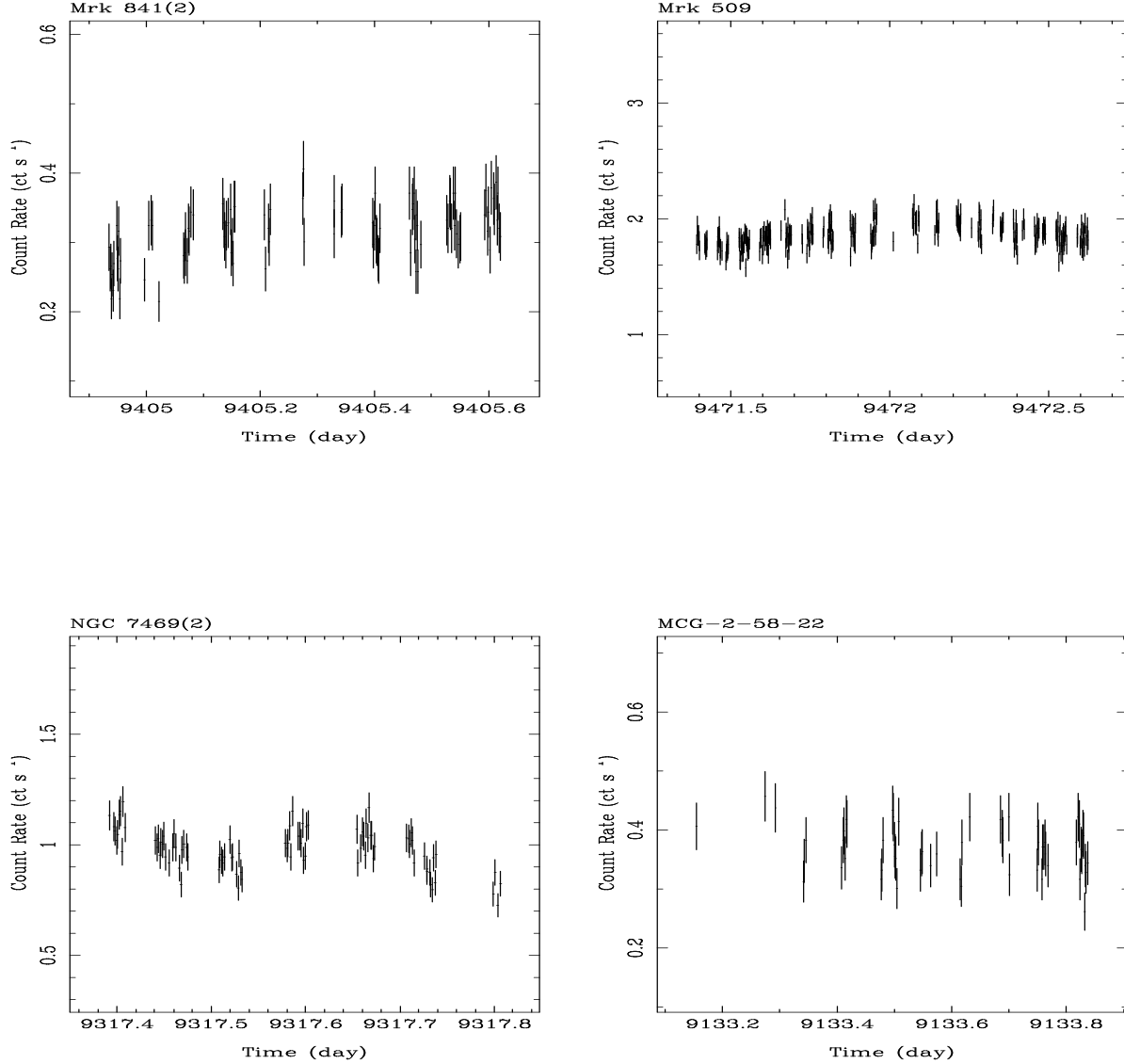


Fig. 3.— Light curves for the sources in our sample, in 128s bins, for the combined SIS data in the 0.4-10 keV range. The time axis is in modified julian date, mJD-40000. NGC 6814 has been excluded due to its low count rate. The y-axis is scaled to the mean value, to allow comparison of the variability amplitudes, with $y_{\max}=2*\text{mean}$ and $y_{\min}=\text{mean}/4$, except for NGC 4051, where the amplitude of variability is so large that we have had to increase these limits by 50 per cent. Most objects show variability on this timescale and also on longer (\sim hr) timescales (see Tables 5 and 7).

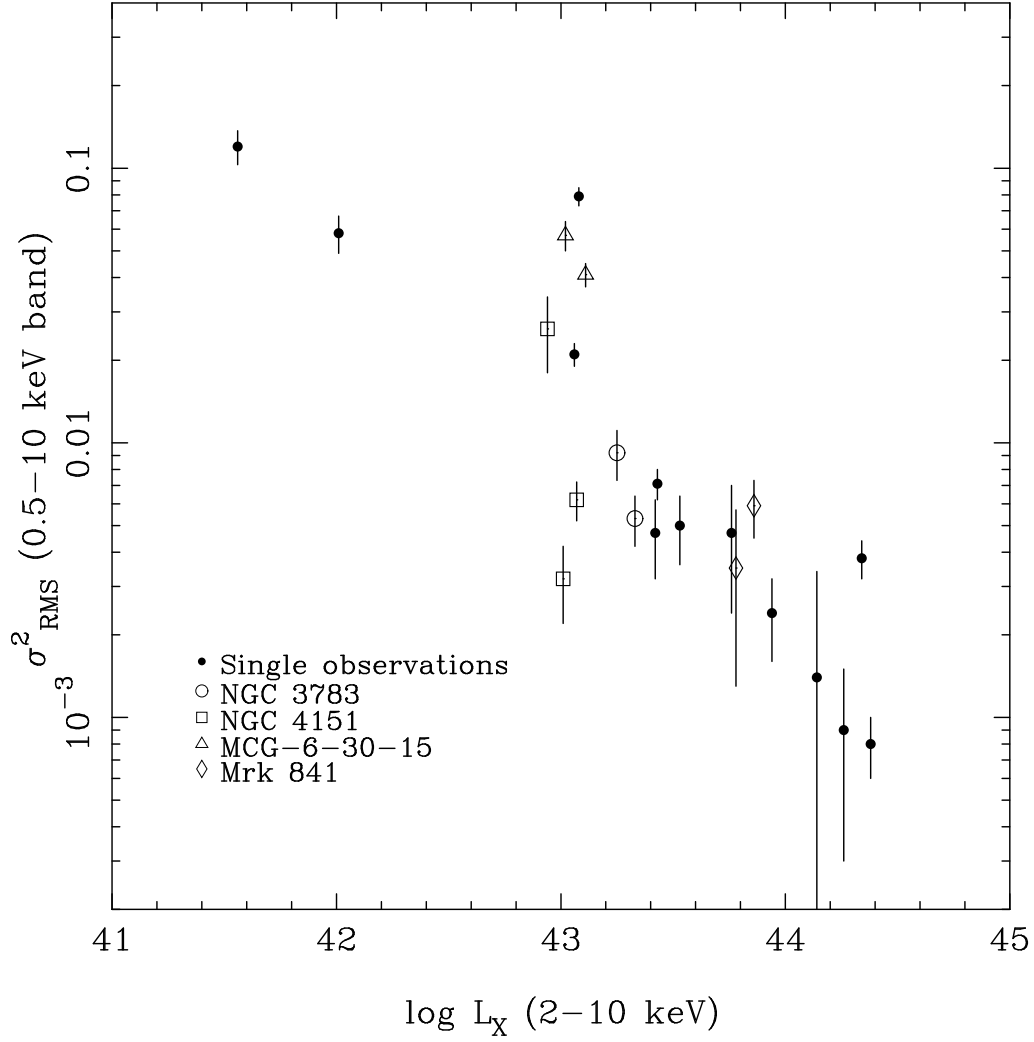


Fig. 4.— Normalized, excess variance (σ_{RMS}^2 versus luminosity. Where there are multiple observations of a source, they have been plotted separately. A highly significant trend of decreasing amplitude is observed with luminosity. Spearman rank and Pearson linear correlations give significances of > 99.9 per cent confidence.

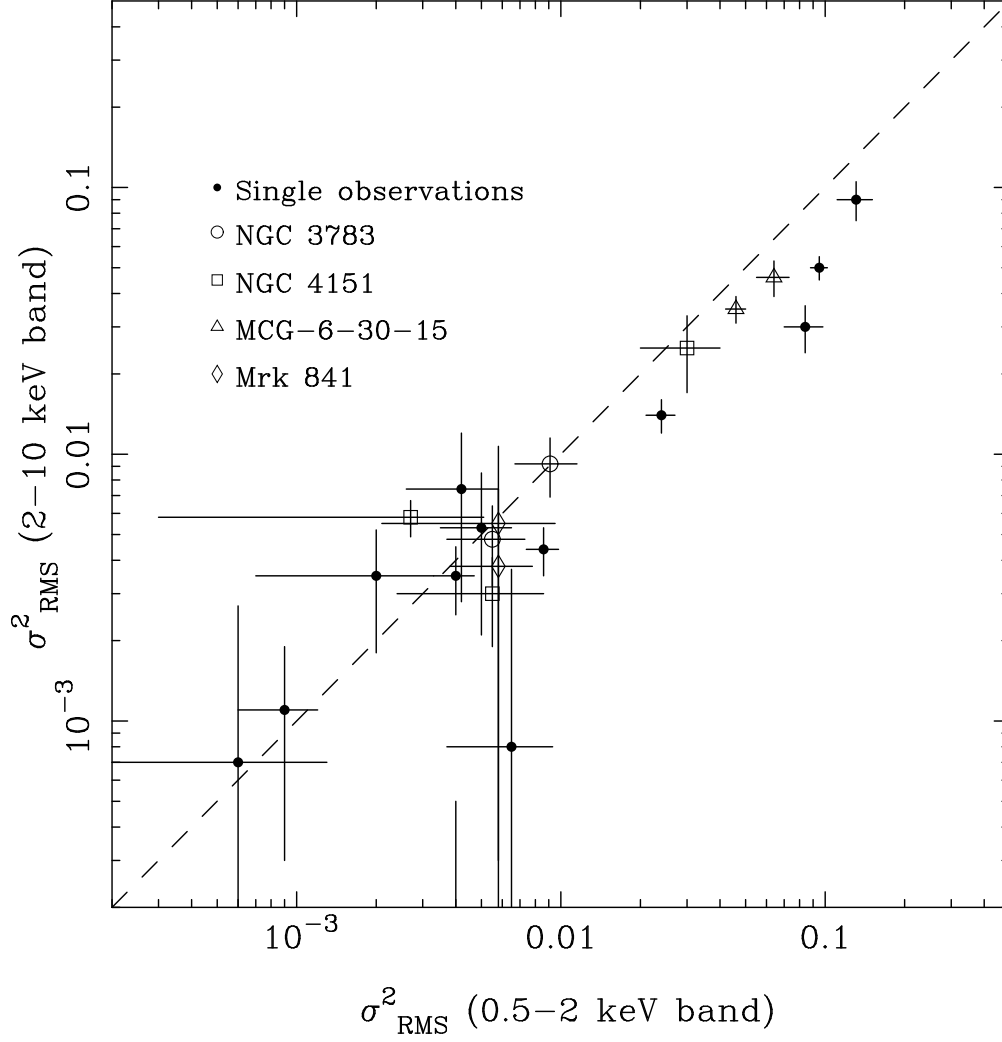


Fig. 5.— σ^2_{RMS} variability amplitude in the soft band (0.5-2 keV) versus that in the hard band (2-10 keV) of the SIS. The dashed line shows a 1:1 relationship. In a number of cases, the amplitude of variability in the soft X-ray band appears to be greater than in the hard X-rays. This implies some spectral variability.